Zoological Journal of the Linnean Society, 2020, **XX**, 1–14. With 9 figures.

Tooth-shape adaptations in aglyphous colubrid snakes inferred from three-dimensional geometric morphometrics and finite element analysis

MAHDI RAJABIZADEH[1,2*], SAM VAN WASSENBERGH[1,3], CHRISTOPHE MALLET[1], MARTIN RÜCKLIN[4] and ANTHONY HERREL[1,3,5]

[1]*UMR7179 CNRS/MNHN, Département Adaptations du vivant, Muséum national d'Histoire naturelle, Paris, France*
[2]*Department of Computer Science, Tarbiat Modares University, Tehran, Iran*
[3]*University of Antwerp, Department of Biology, Functional Morphology, Antwerp, Belgium*
[4]*Naturalis Biodiversity Center, Postbus 9517, 2300 RA Leiden, The Netherlands*
[5]*Ghent University, Department of Biology, Evolutionary Morphology of Vertebrates, Ghent, Belgium*

Received 20 September 2019; revised 16 April 2020; accepted for publication 9 May 2020

To date there are few quantitative studies investigating the evolution of tooth shape and function in aglyphous snakes in relation to diet. A considerable evolutionary decrease in body size is observed in whip snakes of the genus *Dolichophis* and their sister-group *Eirenis*. This was coupled with a considerable shift in diet from a regime consisting mainly of prey with endoskeleton to prey bearing a hard exoskeleton. Three-dimensional (3D) geometric morphometrics revealed that the maxillary and palatine teeth of *E. persicus* are blunt and conical in shape, while the same teeth are sharp and elongated in *E. punctatolineatus* and *D. schmidti*. Blunt and conically shaped teeth, as observed in *E. persicus*, seem to be more adapted for biting hard-bodied, arthropod prey. In contrast, the sharp and elongated teeth in *Dolichophis* and *E. punctatolineatus*, are likely specialized for puncturing prey with an endoskeleton. The results of a finite element analysis confirms that during the biting of a hard-bodied prey, the generated stresses in *E. persicus* teeth are well below the von Mises yield criterion, while in *D. schmidti* the value is roughly two to three times higher, indicating that *E. persicus* teeth are better suited for biting hard-bodied prey such as arthropods.

ADDITIONAL KEYWORDS: dentary – *Dolichophis* – *Eirenis* – maxilla – palatine – pterygoid – reptiles.

INTRODUCTION

Vertebrate teeth refer to highly mineralized structures mainly associated with the ingestion and processing of prey. However, they may also serve other functions such as defence (Koussoulakou *et al.*, 2009). Phylogeny and dietary habits have driven the teeth of vertebrates to acquire numerous anatomical forms and shapes (Knox & Jackson, 2010). Snake teeth are typically recurved, sharply pointed and mainly acrodont, although some are pleurodont, as in scolecophidians (Zaher & Rieppel, 1999). Snakes can be placed in four groups based on their dental morphology, although this grouping does not describe monophyletic groups. Aglyphous snakes, e.g. of the families Boidae, Pythonidae and many colubrid snakes, have a series of more or less similarly shaped, posteriorly curved teeth on the maxillae, without a groove. Opisthoglyphous snakes, e.g. many snakes of the family Lamprophiidae and some colubrids, possess a full row of teeth on the maxillae, including enlarged, grooved (on the mesial or lateral tooth surface), posteriorly curved teeth in the middle of the tooth row or at the back. Proteroglyphous snakes of the family Elapidae have fixed, enlarged teeth on the anterior portion of the maxillae with closed venom grooves, except for an opening near the tip. Solenoglyphous snakes, e.g. family Viperidae and *Atractaspis* of the family Lamprophiidae, have tubular, enlarged, fully closed teeth on the reduced maxillae

*Corresponding author. E-mail: Khosro.rajabizadeh@gmail.com

that can be rotated around the prefrontal (Kardong & Young, 1996; Deufel & Cundall, 2006; Berkovitz & Shellis, 2016). In Aglyphous snakes, which comprise roughly 85% of extant snakes, teeth are considered as not specialized for venom injection, nor to mediate venom penetration into the body of the prey (Berkovitz & Shellis, 2016).

Previous studies have reported structural and functional adaptations in Aglyphous snakes in relation to diet, including the occurrence of numerous long and sharp teeth in some piscivore snakes (Savitzky, 1983), the occurrence of hinged, weakly ankylosed teeth in some lizard- (Savitzky, 1981, 1983) or arthropod-eating snakes (Jackson *et al.*, 1999), the occurrence of teeth that are reduced in size and number in egg-eating snakes (Gans, 1952) or numerous, elongated dentary teeth and reduced palatomaxillary teeth in snail-eating (malacophagous) snakes (Savitzky, 1983). However, to date there are few detailed and quantitative studies investigating the evolution of tooth shape and function in Aglyphous snakes in relation to diet.

A lineage that is of particular interest due to its large range of adult body sizes, coupled with a broad range of prey hardness, is the one including dwarfed snakes of the genus *Eirenis* and their immediate sister-group, whip snakes of the genus *Dolichophis* (Rajabizadeh *et al.*, 2020, in press). *Dolichophis* (maximum size: about 2500 mm) is distributed across southern and eastern Europe, Asia Minor, countries west of the Mediterranean Sea to southern Russia, western Kazakhstan, the Caucasus and the western and northern Iranian Plateau. These snakes inhabit mountainsides and hilly landscapes, and feed on a variety of food items, including small mammals, birds, lizards and, more rarely, on bird eggs, arthropods and even other snakes (Terent'ev *et al.*, 1965; Göçmen *et al.*, 2008; Lelièvre *et al.*, 2012; Rajabizadeh, 2018). *Eirenis* is distributed throughout southern Europe, north-eastern Africa, Asia Minor and countries west of the Mediterranean Sea to the Iranian Plateau. These snakes inhabit mountainsides and hilly landscapes. *Eirenis* is divided into four subgenera, *Eirenis*, *Eoseirenis*, *Pediophis* and *Pseudocyclophis*, which, except for *Eoseirenis*, are more or less dwarfed and feed on lizards and/or arthropods (Rajabizadeh, 2018). *Eirenis* (*Pediophis*) *punctatolineatus* (Boettger, 1892) (maximum size: 758 mm) feeds mainly on lizards and arthropods, while *Eirenis* (*Pseudocyclophis*) *persicus* (Anderson, 1872) (maximum size: 371 mm) feeds nearly exclusively on arthropods (Terent'ev *et al.*, 1965; Rajabizadeh, 2018).

Hence, a considerable evolutionary decrease in size is observed from a *Dolichophis*-like ancestor to the miniature *Eirenis*, coupled with a considerable shift in their diet from a regime consisting mainly of prey with an endoskeleton to prey bearing a hard exoskeleton. Thus, during the evolutionary transformation of *Dolichophis–Eirenis*, a broad range of size decrease is coupled with a broad range of prey hardness increase. We hypothesize that (1) tooth shape in miniature *Eirenis* is different than in *Dolichophis* and (2) tooth shape in *Eirenis* and *Dolichophis* reflect a suite of structural and functional adaptations in relation to prey hardness, allowing them to better resist the strains associated with the biting of prey. To test these hypotheses, we provide a detailed structural and functional comparison of the shape of the teeth in *Dolichophis* and *Eirenis*.

MATERIAL AND METHODS

Specimens

To study the dental adaptations to diet, we examined an adult and a juvenile *Dolichophis schmidti* (Nikolsky, 1909), one *E. persicus* and one *E. punctolineatus*, all of which were micro CT-scanned. A juvenile *Dolichophis* was included in the study to verify whether the difference in tooth shape among the adults of *Dolichophis* and *Eirenis* is a result of size constraints or, alternatively, may reflect adaptation to a different diet. Biometric data of the examined specimens are presented in Table 1.

The micro-CT scans of the heads of the four snake specimens were performed at the Centre for X-ray Tomography of Ghent University (Masschaele *et al.*, 2007). The setup was a transmission head of a dual-head, X-ray tube (Feinfocus FXE160.51) and a-Siflat panel

Table 1. Biometric data, as well as micro-CT scan details, of the examined specimens. Acronyms are as follows: snout–vent length (SVL), tail length (TL) and head length (HL) measured from tip of rostral to end of lower jaw.

Species	SVL (mm)*	TL (mm)	HL (mm)	No. of projections	Voxel size (µm)
Dolichophis schmidti (adult)	750	150	35.2	1762	19.863
Eirenis punctatolineatus	408	136	14.8	1781	11.261
Eirenis persicus	233	66	8.0	1802	6.2
Dolichophis schmidti (juvenile)	380	92	12	1714	7.616

*: Millimeter

detector (PerkinElmer XRD 1620 CN3 CS). The focal spot size was 900 nm at a tube voltage of 130 kV for high resolution. The number of projections and voxel size of the scanned specimen are presented in Table 1. The exposure time was 2 s per projection. The raw data were processed and reconstructed using the in-house CT software 'OCTOPUS' (http://www.octopusreconstruction.com; Vlassenbroeck *et al.*, 2007) and rendered using AMIRA v.5.4.1 (Mercury Systems of Visage Imaging GmbH). The CT-rendered images were colour-coded to distinguish separate ossified units, where stiff and rigidly interconnected bones were given a single colour. CT scan details of the scanned specimens are presented in Table 1.

The palatomaxillary arch and the mandible of each examined specimen were isolated from the rest of the skull using the segmentation tool in AMIRA. Teeth of the left side of the palatomaxillary arch and the left mandible were isolated along a straight line crossing the anterior and posterior edges of the tooth socket and then prepared using Geomagic Wrap v.2017.1. To prepare a tooth for 3D-shape analysis, the basal edges of each tooth were covered by a flat plane, except for the central pulp cavity. Then, each tooth was checked for holes, spikes, self-intersections and non-manifold edges using the Repair Module in Geomagic. The surface noise due to scanning was reduced (mid-smoothness level) using the Smooth Module in Geomagic Wrap. Since snake teeth are replaced regularly, only active teeth (i.e. those fully fused to the socket) were used here.

Morphometrics

A combination of anatomical landmarks and semi-landmarks sliding on both curves and surfaces (Gunz *et al.*, 2005; Gunz & Mitteroecker, 2013) were used to quantify the shape variation of the teeth. A total of 306 landmarks were placed on each tooth, including ten anatomical landmarks and 296 sliding semi-landmarks. Of those, 120 were curve semi-landmarks bordering the base of the tooth, and 176 were surface semi-landmarks distributed homogenously over the tooth surface (Fig. 1).

The anatomic landmarks and semi-landmarks were digitized using the IDAV Landmark software package

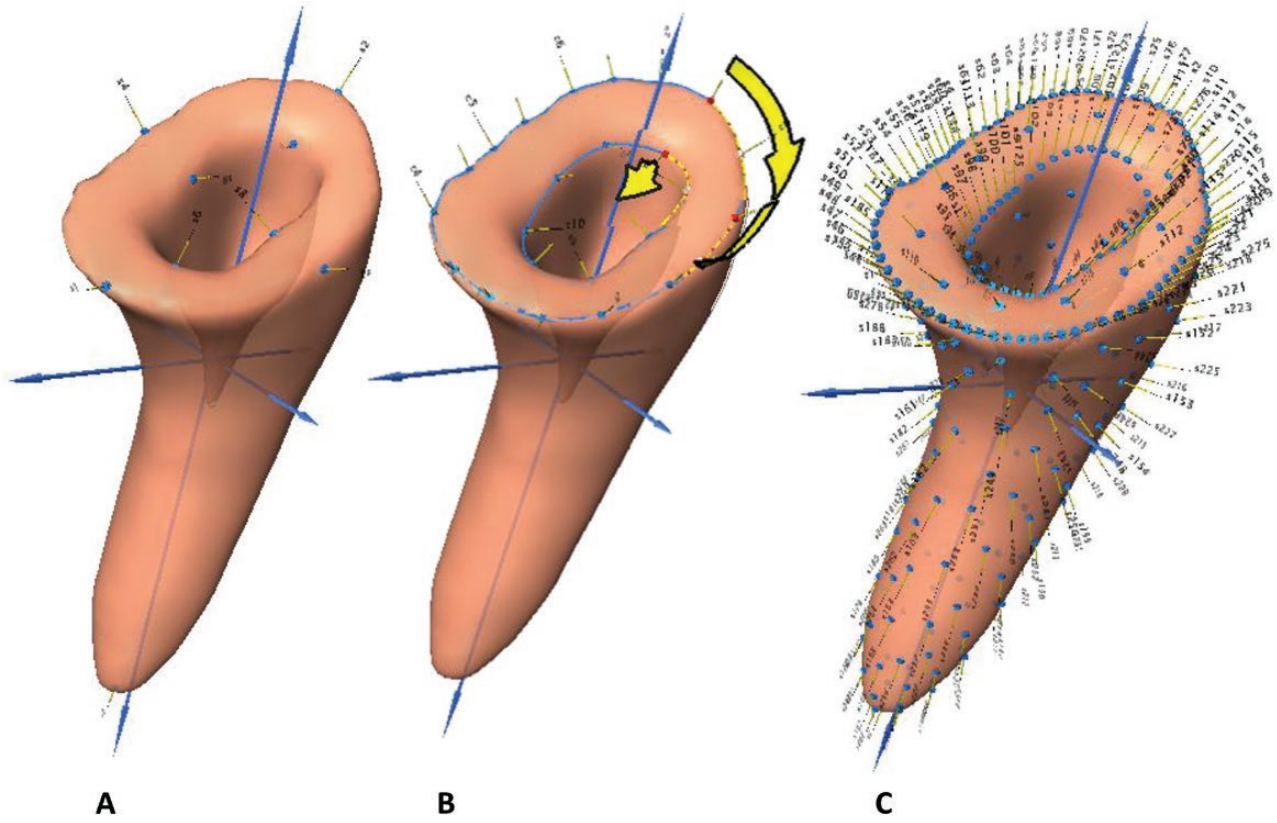

Figure 1. Position of the landmarks on a tooth, including ten anatomical landmarks (A), 120 curve semi-landmarks (eight curves on outer edge of the tooth base, specifying 80 curve semi-landmarks and four curves on inner edge of the tooth pulp specifying 40 curve semi-landmarks (B)) and 176 point semi-landmarks on the tooth surface (C).

(Wiley *et al.*, 2005). Curve-sliding semi-landmarks were equidistantly re-sampled and bordered by anatomical landmarks (Gunz *et al.*, 2005; Botton-Divet *et al.*, 2016). Surface semi-landmarks were digitized manually on the surface of a template tooth mesh using the IDAV Landmark software package. This template was used to project the surface semi-landmarks on to the surface of the examined teeth. As recommended by Gunz & Mitteroecker (2013), curve and surface semi-landmarks were slid to ensure that each point can be considered as spatially homologous. Sliding was done by minimizing the bending energy of a Thin Plate Spline between each specimen and the template at first, and then the Procrustes consensus was used as a reference during the next three iterative steps. The sliding of surface semi-landmarks over the surface of the teeth was performed using the 'Morpho' package (Schlager, 2013) as detailed in Botton-Divet *et al.*, (2015). Both curve and surface semi-landmarks were slid using the bending energy minimization criterion.

A generalized Procrustes analysis was performed using the 'Morpho' R package (Schlager, 2013). Shape variation was visualized using a principal component analysis (PCA), performed on the superimposed coordinates projected onto the tangent space, using 'Morpho' R package (Schlager, 2013). The analyses were performed in R (R Core Team, 2016).

Non-parametric multivariate analysis of variance of the landmark data were used to evaluate significant differences among each group (for maxillary, palatine, pterygoid and dentary teeth separately). As a proxy of quantitative shape divergence among the teeth of the examined snakes, we calculated the Euclidean Distances between the centroid PC scores. To do so, the average PC scores on the first and second PC were extracted. Subsequently the distance between the PC scores was computed using the following formula:

$$D = \sqrt{\sqrt{(x2\ \ x1)2 + (y2\ \ y1)2}}$$

In which $(x1, y1)$ is the Euclidean coordination of the first point and $(x2, y2)$ is the Euclidean coordination of the second point.

Finite element analysis (FEA)

To evaluate the effect of tooth shape on its resistance to the deformations imposed during biting a hard prey, a finite element analysis (FEA) was performed. In this analysis, we focused on maxillary teeth, because (1) a clear difference in the shape of maxillary teeth was documented between *E. persicus* and the rest of the examined specimens, (2) some data are available to evaluate the movement of the maxillary bone during biting (Cundall, 1983; Schwenk, 2000) and (3) muscular structures involved in maxillary biting are straightforward, simplifying the orientation of the external forces acting on the maxilla.

Geometry preparation

The mean shape of the maxillary teeth of *D. schmidti* and *E. persicus* was selected based on the PC scatter plot. So, in each species, regarding the Euclidean distribution of maxillary teeth across the PC1 vs. PC2 scatter plot, the tooth located closer to the middle of this distribution was selected. Hence, the 8th maxillary tooth of *E. persicus* and the 5th maxillary teeth of *D. schmidti* (both on the left maxilla) were selected as the maxillary tooth mean shape. The mean shape was trimmed using Fix Module in 3-Matic Medical v.11 (Materialise, Leuven, Belgium).

Meshing

Finite element analysis begins by dividing a structure into a mesh of discrete elements that together approximate the geometry of the structure being modelled. Each element is assumed to have specific material properties that empirically relate the deformation (stress) of an individual element to the applied load (stress) at the element boundaries (Faulkner *et al.*, 1991). It is important to evaluate mesh convergence studies in order to obtain the required mesh size in creating the FEA models (Ahmad *et al.*, 2013). To calculate the proper mesh size, a convergence analysis was performed on the maxillary tooth mean shape of *E. persicus*. For this analysis, 0.00024 N was implemented along the main axis of the tooth, over three outermost nodes on the tip of the tooth. Constraint and loading conditions are explained in a following section. The resulting plot shows the element size against the maximum computed stress (von Mises) and confirmed that the variation around the element size equal to 0.01 mm does not affect the resulting stress values drastically (Fig. 2). Using an element size of 0.01 mm, the maxillary tooth mean shape of *E. persicus* was meshed with 7176 tetrahedral elements and the maxillary tooth mean shape of *D. schmidti* was meshed with 13 052 tetrahedral elements. Both the meshes generated with the default growth rate of 1.2, using Meshing Module of ANSYS v.15.0 0 (ANSYS, Canonburg, PA, USA).

Material properties

Despite extensive data on the material and mechanical properties of human teeth (Zhang *et al.*, 2014), little is known about the material properties of teeth in other vertebrates. Teeth have been shown to be

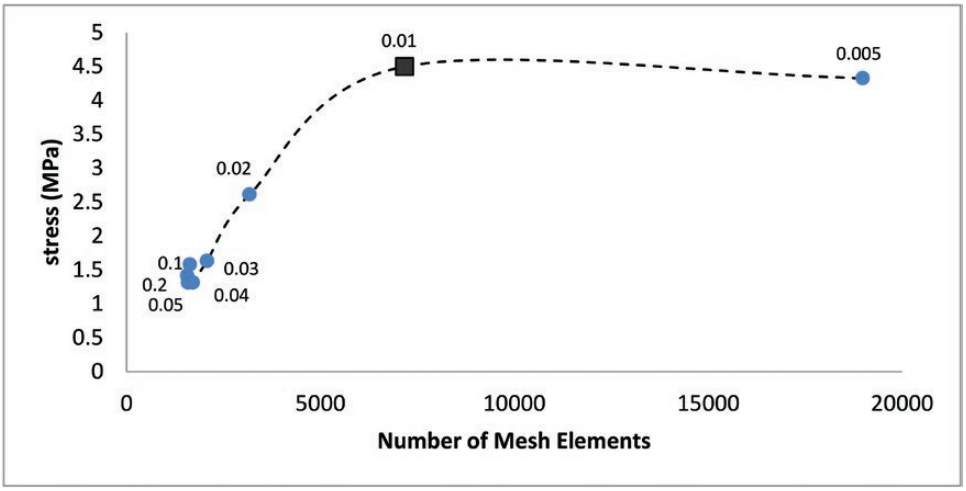

Figure 2. Mesh convergence analysis on the maxillary tooth mean shape of *Eirenis persicus* plotting the element number against the maximum computed stress (von Mises stress, presented in Megapascal). Respected element size is noted over the points. The square represents the element size equal to 0.01 mm.

anisotropic (Waters, 1980) and a complex structure of enamel and dentine layers has been reported in reptiles (Zahradnicek *et al.*, 2014). However, data concerning the thickness and distribution of enamel and dentine are not available for the examined colubrid snakes. Hence, and because of the comparative nature of our model, we considered the examined teeth as static, linearly elastic, isotropic and homogenous, for the sake of model simplicity. Moreover, Jansen van Vuuren *et al.* (2016) studied the composition of dental tissues in elapid and viperid snakes and concluded that snake fang and human tooth dentin are chemically and mechanically similar. Hence, we used the data available for human dentine: Young's modulus (E = 18 000 MPa) and Poisson's ratio (v = 0.31) (Bessone *et al.*, 2014).

Constraint, forces and loading condition

The application of the realistic forces and constraints are essential for successful FEA modelling (Dumont *et al.*, 2005). In *Dolichophis* and *Eirenis*, prey ingestion (defined as the first step in snake feeding that involves capturing or biting of the prey, not swallowing it) is mainly performed by the maxilla. Each maxilla is a curved bone, posteriorly connected to the ectopterygoid and medially articulated with the ventral surface of the prefrontal. Hence, the maxilla is a movable bone, with a degree of rotation along the medial articulation with the prefrontal. Maxilla movement, including the downward movement needed to bite the prey (Fig. 3C) and the subtle rotation along the posterior junction with ectopterygoid and medial articulation with the ventral surface of the prefrontal, results from the contraction of pterygoideus and pterygoideus accessories muscles (Fig. 3) (Kardong *et al.*, 1986). During prey capture, the maxillary teeth slide over the prey to align forces acting on the teeth with the long axes of the teeth (Schwenk, 2000). Hence, in the movable maxilla, a range of orientations of the forces acting around the main axis of a maxillary tooth can be expected (Fig. 3). Given the above-mentioned condition, we set up the model as follows:

- *Constraint:* the external nodes on the tooth base were designated as fixed to constrain both the translational and rotational displacement.
- *Force:* in *Eirenis persicus*, maximal force generated by pterygoidous and pterygoideus accessories muscles was calculated as 0.19 N (Rajabizadeh *et al.*, 2020). Since in the current study, the left maxillary bone of *E. persicus* has eight active teeth, firmly attached to the maxilla, and assuming that all teeth are in contact with the food item during the ingestion, a force of 0.024 was applied to each tooth.
- *Loading condition:* the force was distributed over the outer surface of the tip of the tooth. Considering the geometry and sharpness of the teeth, the force was implemented over 75 nodes on tip of

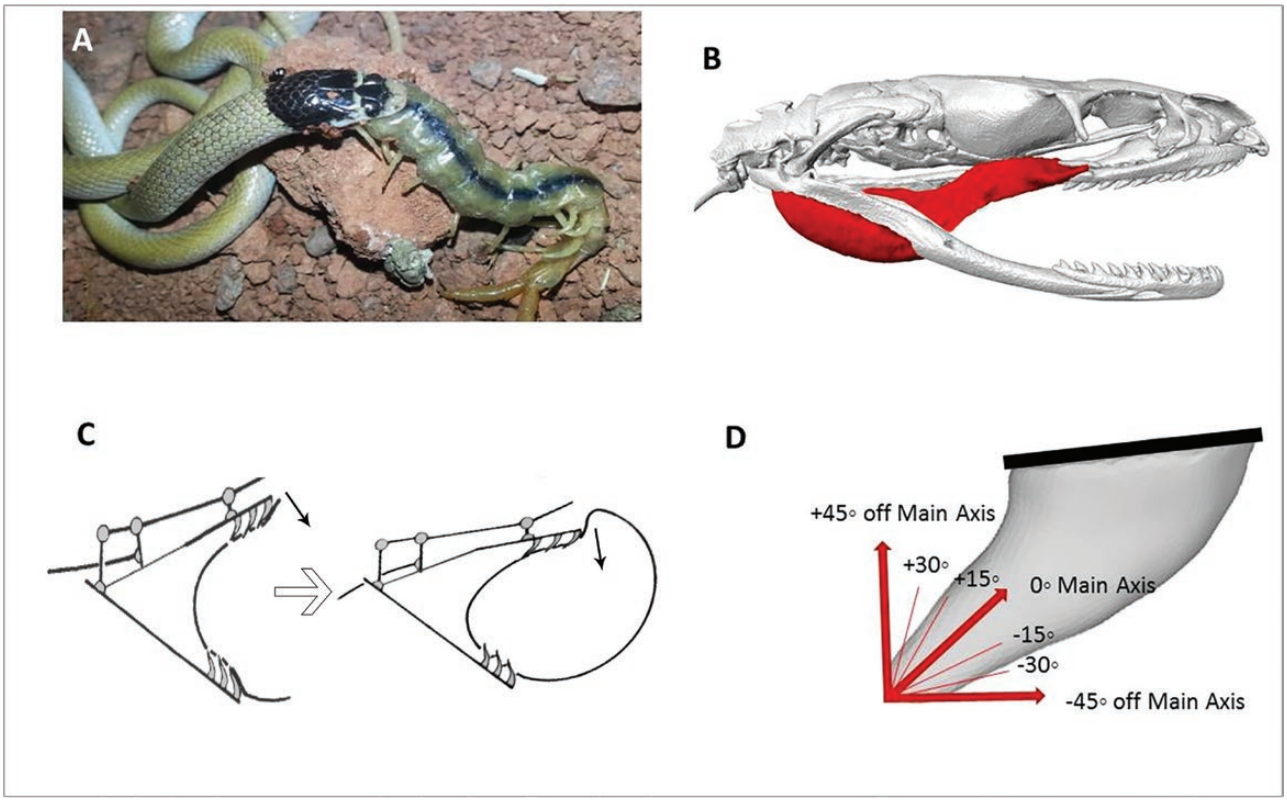

Figure 3. A, feeding of *Eirenis persicus* on a centipede: a massive, elongated arthropod (photo by S. Sami). B, anatomical position of the pterygoideus and pterygoideus accessories muscles that generate the movement of the maxilla. C, schematic presentation of snake ingestion, showing maxilla movement direction (small arrows) and maxillary teeth sliding over the prey to align the forces acting on the teeth with the long axes of the teeth. D, a range of forces acting in the sagittal plane including the main axis of the tooth, as well as ± 45º off the main axis, with the intervals of 15º was implemented.

the *E. persicus* tooth and 31 nodes on tip of the *D. schmidti* tooth. The direction of the force was set up along the sagittal surface of the tooth, across the main axis of the tooth, as well as ± 45° off the main axis, at 15° intervals (Fig. 3).

Finite element analysis (FEA) model

The FEA was performed using a Static Structural Module in ANSYS v.15.0 (ANSYS, Canonburg, PA, USA). To compare the structural strength of an *E. persicus* and a *D. schmidti* maxillary tooth of mean shape in response to the stress caused during biting, the von Mises stress distributions were investigated. Von Mises stress is widely accepted for identifying the potential location of the failure due to the stress concentrations in biological structures (Dumont *et al.*, 2005; Whitenack *et al.*, 2011). To be able to compare the von Mises values independent of size differences, the maxillary tooth of *D. schmidti* was scaled to the volume of an *E. persicus* tooth, and then the constraints, forces and loading conditions, described above, were implemented for both of the examined teeth.

Fatigue analysis

To check the sensitivity of the tooth to force during repeated loading cycles, we also performed a fatigue analysis. Constraints, forces and loading conditions were set up as defined above, along the main axis of the tooth, but the magnitude of the force was changed from 50% of the defined load, up to 150% of the defined load. The fatigue curve of human dentin was generated based on a study by Nalla *et al.* (2003). The resulted fatigue sensitivity chart indicates how fatigue results change as a function of the force magnitude implemented at the tip of the tooth. Fatigue analysis was performed using the Fatigue Tools Module of ANSYS v.15.0 0 (ANSYS, Canonburg, PA, USA).

RESULTS

Shape analysis

Bonferroni-corrected *P*-values resulting from the non-parametric multivariate analysis of variance of the landmark data of the examined teeth reveal that each group of the teeth (maxillary, palatine, pterygoid and dentary) is significantly different among the examined snakes (except the palatine teeth of the adult *D. schmidti* and *E. punctatolineatus*, the pterygoid teeth of the juvenile *D. schmidti* and *E. persicus* and the dentary teeth of the adult *D. schmidti*, which are similar to the dentary teeth of the other examined specimens) (Supporting Information, Table S1). The PCA scatter plots of the landmark data for the maxilla, palatine, pterygoid and dentary teeth in the examined specimens are presented in Figure 4. Maxilla and palatine teeth of *E. persicus* are blunt and conical in shape, and show clear differences from the sharp and elongated maxillary and palatine teeth of *E. punctatolineatus*, as well as those of the adult and juvenile *D. schmidti*. A similar difference can be noted for the pterygoid teeth. In contrast, the dentary teeth are not as different (Fig. 4). The scatter plot resulting from PC1 vs. centroid size of the teeth indicates that the observed divergence in PC1 does not simply reflect size differences, but also differences in the shape of the teeth (Fig. 4). The pairwise Euclidean distance of the centroid PC scores of the maxilla, palatine, pterygoid and dentary teeth (Fig. 5; values in Supporting Information, Table S2) reveals that the lowest shape divergence exists among the adult and juvenile *Dolichophis*, while the highest shape divergence is observed between the pterygoid teeth of *E. persicus* and *E. punctatolineatus*. In comparison, *Dolichophis* (both adult and juvenile) differs from *E. punctatolineatus*, respectively, in the shape of the pterygoid, dentary, maxilla and palatine teeth, in a decreasing order. *Dolichophis* (both adult and juvenile), when compared with *E. persicus*, shows the highest shape divergence in a decreasing order among the maxilla, pterygoid, palatine and dentary teeth, although the difference between palatine and dentary teeth of the adult *D. schmidti* and *E. persicus*, as well as between the pterygoid teeth of the juvenile *D. schmidti* and *E. persicus*, are not significant.

Finite element analysis (FEA)

When loaded at the tip, both types of teeth (the mean shape of the maxillary teeth of *D. schmidti* and *E. persicus*), regardless of their morphology, show the maximum stress at the tip of the teeth (site of loading). While the maximum von Mises stress in the maxillary teeth in *E. persicus* ranges between 41.6 MPa (along –30° of the tooth main axis) and 64.0 MPa (along +45°), for *D. schmidti* the stress ranges between 106.2 MPa (along +15° of the tooth main axis) and 173.2 MPa (along –45°) (Fig. 6). In both teeth, the minimum deformation is observed while implementing the force along the main axis of the tooth, while the maximum deformation is observed along the +45° (Fig. 7). In both teeth, the stress is more or less restricted to the tip of the teeth while implementing the force along the main axis of the teeth. However, implementing the force along the positive or negative direction leads to confined distribution of stress in the *E. persicus* tooth, but widely distributed stress in the *D. schmidti* tooth (Fig. 8).

The fatigue sensitivity chart (Fig. 9) indicates that the lifecycle of *E. persicus* teeth is nearly constant when the force magnitude implemented to the tip of the tooth changes from 50% to 150% of the defined force and is 235 000 cycles (except for 150% where it is 233 970). However, for *D. schmidti* the tooth is sensitive to the defined force magnitude and when the force exceeds 60% of the defined force, the lifecycle of the tooth drastically reduces. Hence, at the point of the defined force, the lifecycle of the tooth reduces to around 4883 cycles and around 120% of the defined force, the lifecycle of the tooth falls to zero.

DISCUSSION

The morphology of an organism is controlled by the interaction between historical factors and selective pressures (Losos & Miles, 1994). Variation in the shape observed in the dentary and palatomaxillary teeth of *Dolichophis* and *Eirenis* suggests that variation in diet may drive the shape adaptation of the teeth (Knox & Jackson, 2010). However, the adaptive nature of the dentary and palatomaxillary teeth in the examined snakes can only be evaluated based on analyses of their function during feeding.

The first step when snakes are feeding is the ingestion of the prey, which is performed mainly by the maxillary teeth. The contraction of pterygoidous muscle retracts the maxilla, coupled to an elevation of the mandible via the external and internal adductor muscles (Cundall, 1983; Schwenk, 2000). Sharp and elongated maxillary teeth, as observed in *Dolichophis* and *E. punctatolineatus*, are specialized for puncturing or lacerating the skin of prey, causing bleeding (Platt, 1967; Kroll, 1976; Kardong, 1979, 1980). These kind of teeth are also observed in piscivorous snakes (Savitzky, 1983) and are similar to the specialized fangs of proteroglyphous, solenoglyphous and opisthoglyphous snakes (Berkovitz & Shellis, 2016).

Shortened, blunt and conically shaped maxillary teeth, as observed in *E. persicus*, seem to be more adapted for biting hard-bodied arthropod prey. Highly

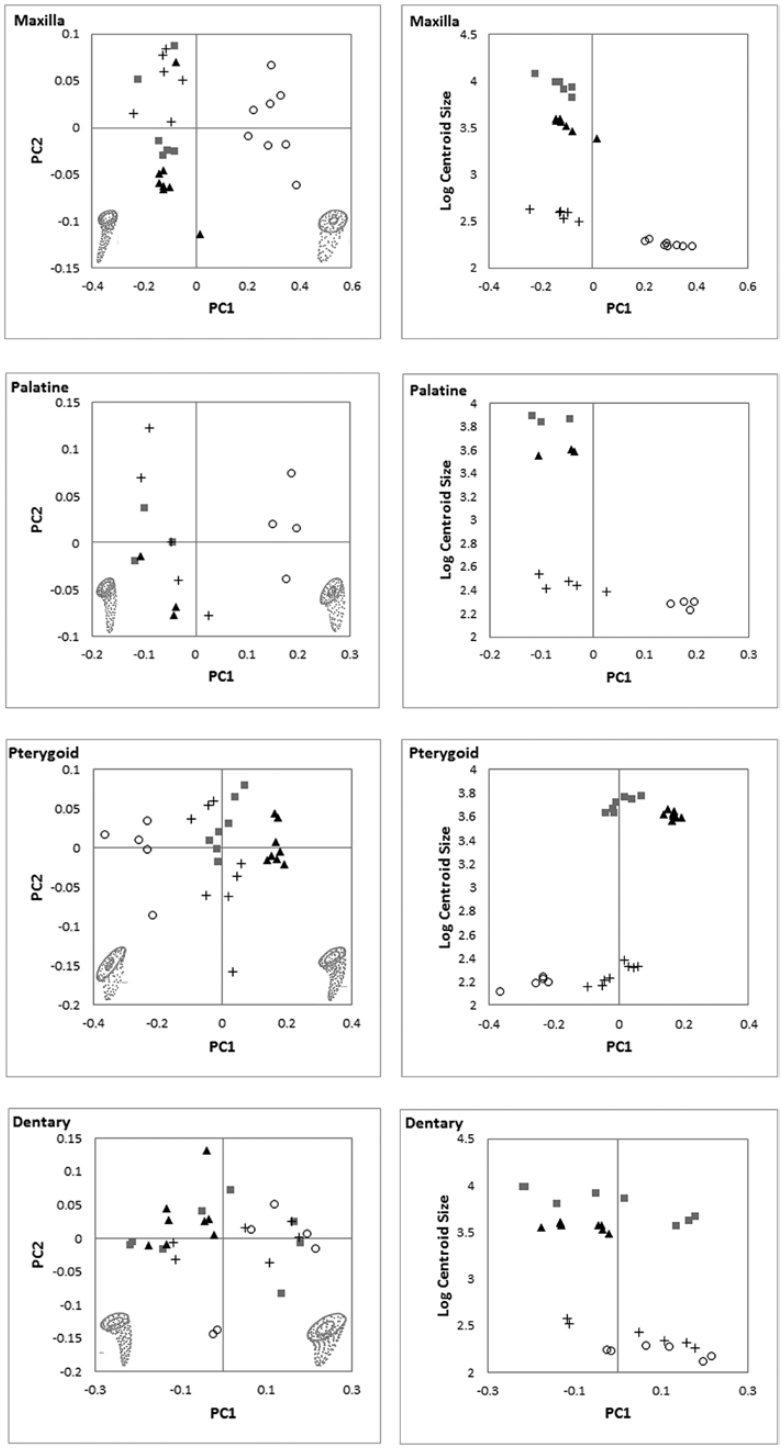

Figure 4. Scatter plots resulting from the principal component analysis on landmark data of teeth of maxilla, palatine, pterygoid and dentary bones in the adult *Dolichophis schmidti* (square), juvenile *D. schmidti* (plus), *Eirenis punctatolineatus* (triangle) and *E. persicus* (circle).

shortened (vestigial) and blunt teeth are observed in egg-eating snakes (Gans, 1952). In addition, blunt, molariform dentition, associated with durophagy, has been observed in molluscivorous lizards, e.g. some amphisbaenians (Pregill, 1984), *Chamaeleolis* lizards (Herrel & Holanova, 2008), northern caiman lizards

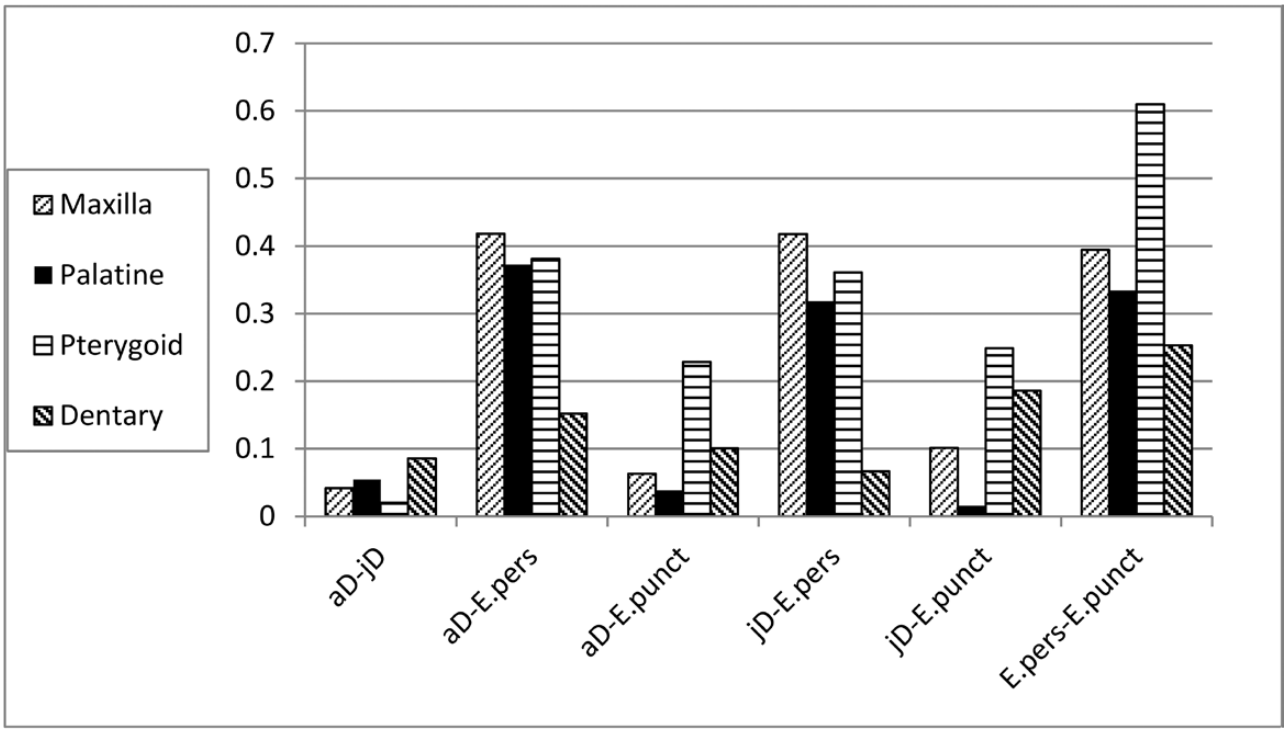

Figure 5. Pairwise Euclidean distance for the maxilla, palatine, pterygoid and dentary teeth in the adult *Dolichophis* (aD), juvenile *Dolichophis* (jD), *Eirenis punctatolineatus* (E.punct) and *Eirenis persicus* (E. pers).

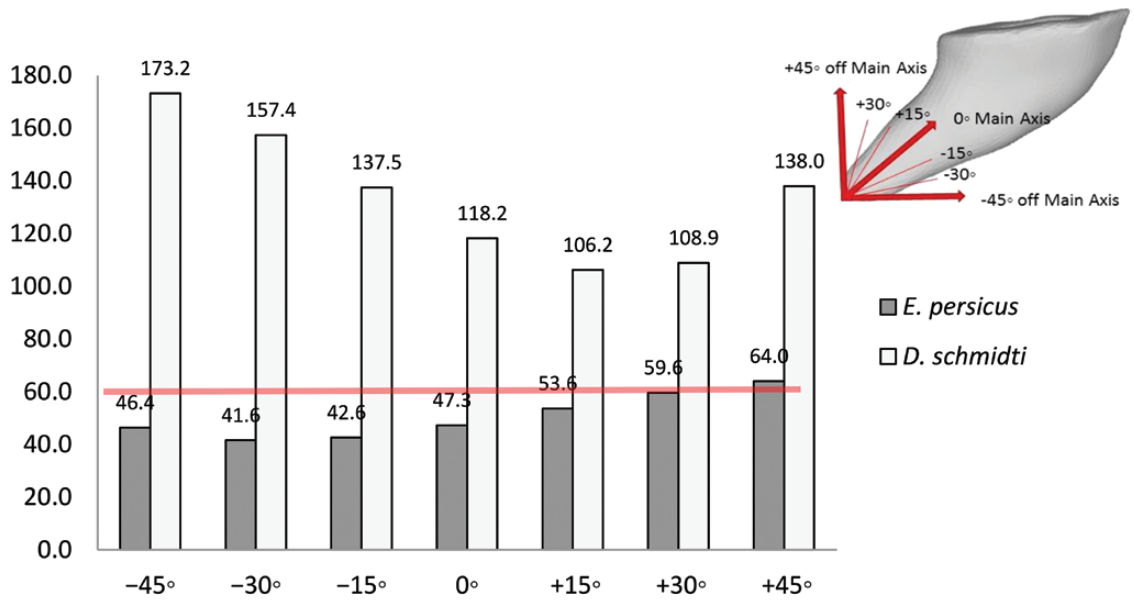

Figure 6. Variation of maximum von Mises stress during loading on tip of the examined mean shape tooth along the main axis of the tooth as well as ± 45° off the main axis with intervals of 15°. The red line indicates to von Mises yield criterion of superficial dentin (= 61.6) (Giannini *et al.*, 2004).

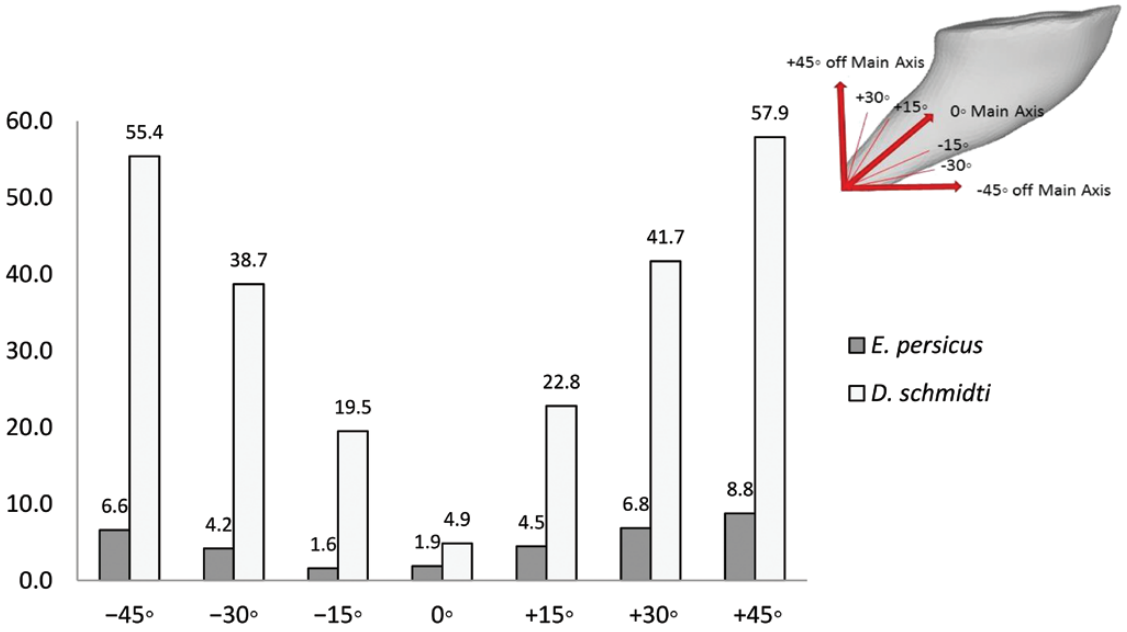

Figure 7. Variation of total deformation (values are in mm and has been multiplied by 10^5) during loading on tip of the examined mean shape tooth along the main axis of the tooth as well as ± 45° off the main axis with intervals of 15°.

(*Dracaena guianensis* Daudin, 1802) (Dalrymple, 1979) and Nile monitors [*Varanus niloticus* (Linnaeus, 1766)] (Rieppel & Labhardt, 1979). Despite some discussion about whether feeding on arthropods should be regarded as durophagy (Savitzky, 1983), the mechanical properties of the exoskeleton of some prey eaten by *Eirenis* likely put constraints on tooth shape.

The results from our biomechanical modelling confirm that during biting the generated stresses in *E. persicus* are mostly confined to the tip of the tooth and mostly well below the von Mises yield criterion of human dentine (61.6 MPa; Giannini *et al.*, 2004). Moreover, our fatigue analysis indicates that *E. persicus* teeth have a high lifecycle duration and likely do not break during biting. In contrast, *D. schmidti* teeth appear less suited for biting hard prey since the generated stresses in the tooth are with values that are roughly two to three times higher than the von Mises yield criterion of the dentine if its teeth would be subjected to the same forces as those of *E. persicus*. The fatigue analysis further indicates that teeth in *D. schmidti* have a low life duration when biting and may actually break when loaded similar to those of *E. persicus*.

During ingestion and swallowing, the mandible elevates to keep the prey pressed against the mouth roof, including the palatomaxillary bar (Cundall, 1983; Cundall & Deufel, 1999; Schwenk, 2000). A lower degree of specialization was observed among the dentary teeth in the examined snakes, suggesting a similar role in pushing the prey against the upper tooth rows while preventing escape.

In colubroids, swallowing the prey is performed via intraoral transport driven by the fore–aft movement of the medial upper jaws (palatine and pterygoid), coupled with the action of the maxilla and lower jaw (Schwenk, 2000). Intraoral transport implies a coordinated advancing of the jaw over the prey through the action of the protractor and levator muscles on one side, and then clamping down on the prey followed by a retraction of the palate–maxillary unit. Next, the process is repeated on the other side, resulting in the characteristic pterygoid walk of snakes. Teeth are important to lock the medial upper jaw teeth on to the prey surface (Cundall, 1983). Similar to maxillary teeth, palatine and pterygoid teeth are also short, blunt and conically shaped in *E. persicus*, possibly an adaptation for biting and clamping down on arthropod exoskeletons without breaking. Whereas the short and blunt palatopterygoid teeth of *E. persicus* resist loading well, the elongated and sharp teeth in *E. punctatolineatus* and *Dolichophis* are likely more efficient in penetrating the skin of small vertebrate prey.

The toughness of food plays a crucial role in shaping teeth (Lucas, 2004). Besides the above-mentioned examples in snakes, well-known examples of dental adaptations to prey hardness have been documented in other vertebrates. Herrel *et al.* (2004) reported tooth-shape difference in omnivorous lacertid

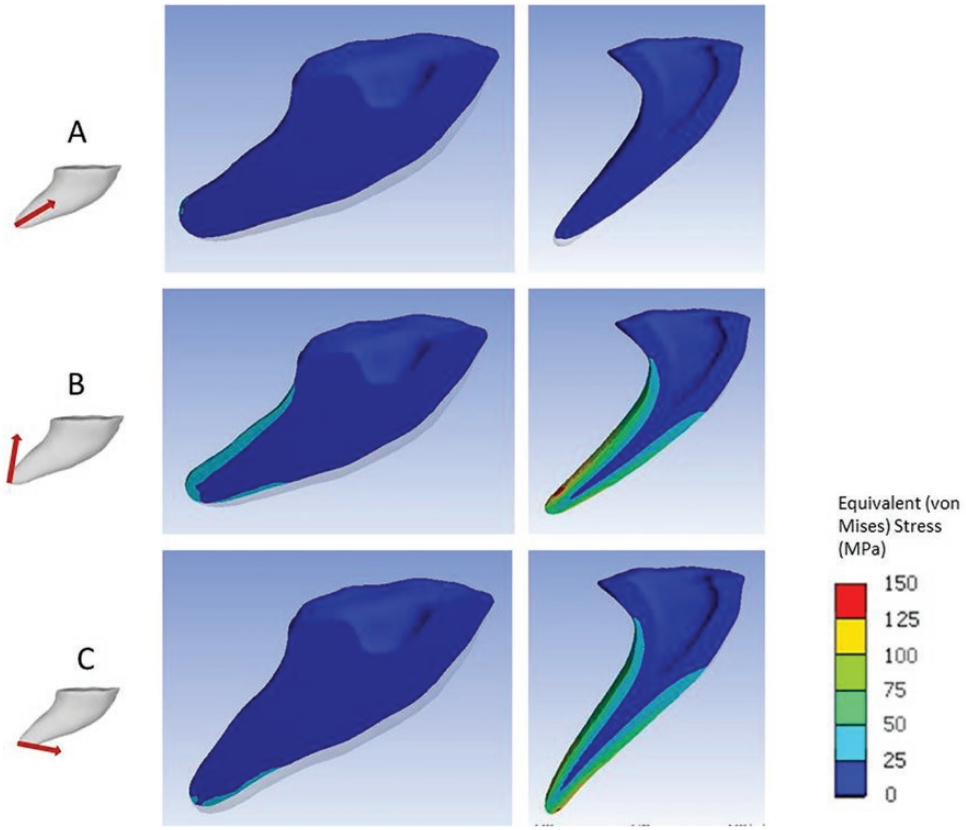

Figure 8. Sagittal surface of *Eirenis persicus* (left) and *Dolichophis schmidti* (right) mean shape maxillary teeth, showing the stress distributions (von Mises) resulting from the force loaded to the tip of the tooth along (A) the main axis of the tooth, (B) +45° and (C) –45° off the main axis.

lizards, *Gallotia galloti* (Oudart, 1839), compared to the insectivorous *Lacerta bilineata* Daudin, 1802. Omnivores have wider teeth with a larger number of cusps, hence a larger tooth perimeter and surface area when compared with insectivores. Blunt molariform teeth are also observed in the snail-crushing teiid lizard genus *Dracaena*, snail-eating amphisbaenid lizards and chamaeleolis lizards, important to avoid tooth breakage while handling a snail (Herrel & Holanova, 2008). Finite element analyses on shark teeth (Whitenack *et al.*, 2011) and spider fangs (Bar-On *et al.*, 2014) revealed that teeth loaded from the tip localized the stress concentrations at the cusp apex. In a unicuspid tooth, smoothed tips of the tooth, without any sharp tips or projection (as observed in *Dracaena* and chamaeleolis lizard, snail-eating amphisbaenid or *E. persicus*), reduce the likelihood of chipping teeth (Lawn *et al.*, 2013). An increased tip surface of the tooth, via larger number of short, thick, cusps (as observed in *Gallotia galloti*), reduces the likelihood of tooth tip failure while loading with a hard prey (Crofts, 2015). Simulations on spider fangs clearly showed that the conical shape of the fang is highly adaptive and improves stiffness and provides damage resilience while biting (Bar-On *et al.*, 2014).

In conclusion, teeth in aglyphous snakes show adaptations in relation to prey hardness. In aglyphous snakes feeding solely on arthropods, such as *Eirenis persicus*, the occurrence of a conical shape and blunt maxillary, palatine and pterygoid teeth are dentary adaptations to resist the tension during the biting of prey with a hard exoskeleton. This adaptation is different from the elongated and sharp palate–maxillary teeth in snakes feeding on prey with an endoskeleton or a mix of prey.

ACKNOWLEDGEMENTS

We are grateful to Dominique Adriaens and Barbara de Kegel from Ghent University and

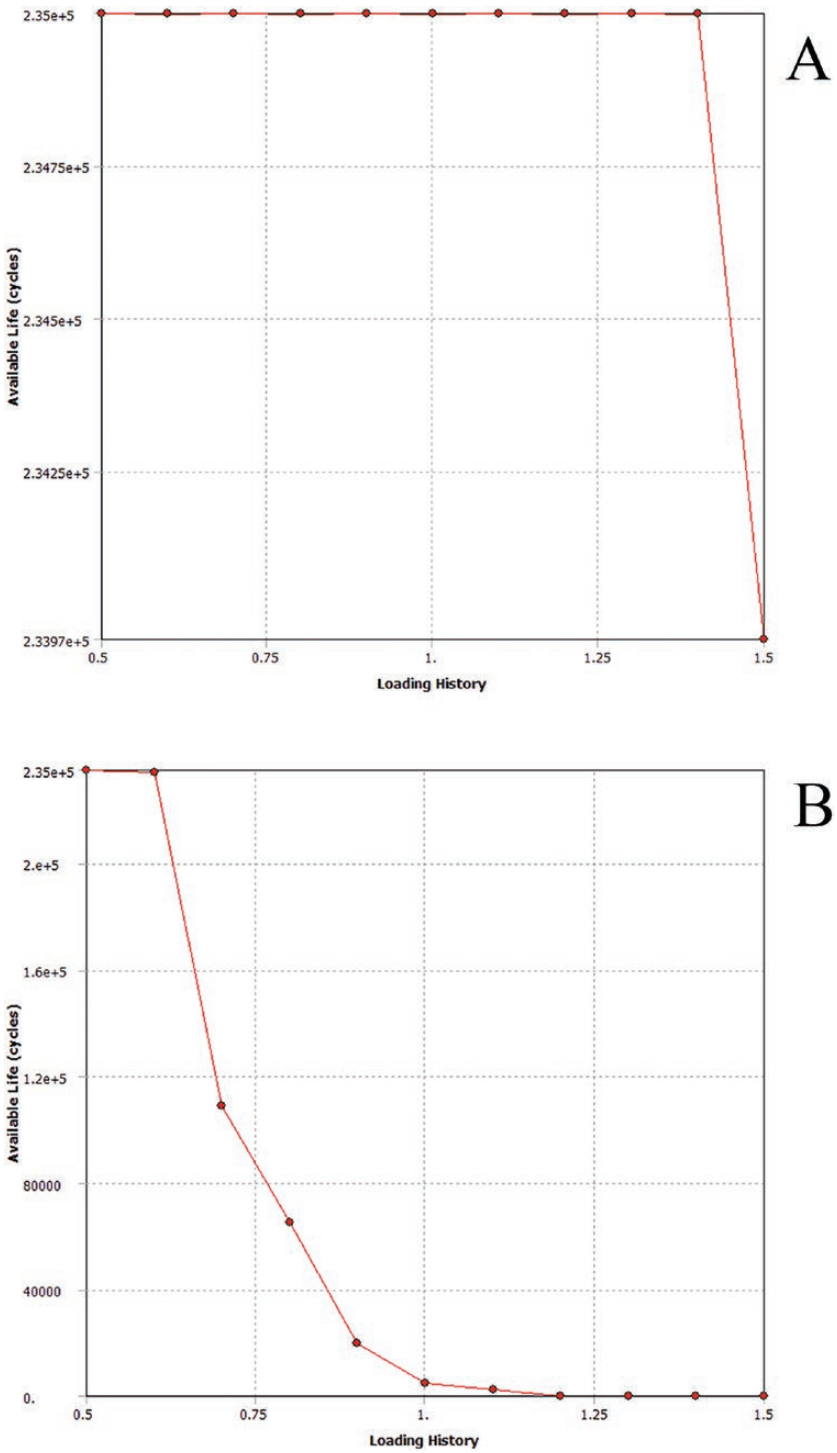

Figure 9. Fatigue sensitivity charts of (A) *Eirenis persicus* and (B) *Dolichophis schmidti* when implementing the force along the main axis of the tooth.

Nasrullah Rastegar-Pouyani from Razi University for their kind collaboration. MR thanks the French Embassy in Tehran for a postdoc grant (2018) that allowed him to work at the MNHN in Paris, as well as the Naturalis Biodiversity Center, Leiden, The Netherlands for a Martin Fellowship grant (2016). Martin Rücklin is funded by Nederlandse Organisatie voor Wetenschappelijk Onderzoek

(NWO) Vidi grant no. 864.14.009. We thank the anonymous reviewers for their careful reading of our manuscript and their many constructive comments.

REFERENCES

Ahmad M, **Ismail K**, **Mat F. 2013.** Convergence of finite element model for crushing of a conical thin-walled tube. *Procedia Engineering* **53:** 586–593.

Bar-On B, **Barth FG**, **Fratzl P**, **Politi Y. 2014.** Multiscale structural gradients enhance the biomechanical functionality of the spider fang. *Nature Communications* **5:** 3894.

Berkovitz BK, **Shellis RP. 2016.** *The teeth of non-mammalian vertebrates.* Cambridge: Academic Press.

Bessone LM, **Bodereau EF**, **Cabanillas G**, **Dominguez A. 2014.** Analysis of biomechanical behaviour of anterior teeth using two different methods: finite element method and experimental tests. *Engineering* **6:** 148.

Botton-Divet L, **Houssaye A**, **Herrel A**, **Fabre A-C**, **Cornette R. 2015.** Tools for quantitative form description; an evaluation of different software packages for semi-landmark analysis. *PeerJ* **3:** e1417.

Botton-Divet L, **Cornette R**, **Fabre A-C**, **Herrel A**, **Houssaye A. 2016.** Morphological analysis of long bones in semi-aquatic mustelids and their terrestrial relatives. *Integrative and Comparative Biology* **56:** 1298–1309.

Crofts S. 2015. Finite element modeling of occlusal variation in durophagous tooth systems. *Journal of Experimental Biology* **218:** 2705–2711.

Cundall D. 1983. Activity of head muscles during feeding by snakes: a comparative study. *American Zoologist* **23:** 383–396.

Cundall D, **Deufel A. 1999.** Striking patterns in booid snakes. *Copeia* **1999:** 868–883.

Dalrymple G. 1979. On the jaw mechanism of the snail-crushing lizards: *Dracaena* Daudin 1802 (Reptilia, Lacertilia, Teiidae). *Journal of Herpetology* **13:** 303–311.

Deufel A, **Cundall D. 2006.** Functional plasticity of the venom delivery system in snakes with a focus on the poststrike prey release behavior. *Zoologischer Anzeiger, a Journal of Comparative Zoology* **245:** 249–267.

Dumont ER, **Piccirillo J**, **Grosse IR. 2005.** Finite-element analysis of biting behavior and bone stress in the facial skeletons of bats. *The Anatomical Record Part A: Discoveries in Molecular, Cellular, and Evolutionary Biology* **283:** 319–330.

Faulkner KG, **Cann CE**, **Hasegawa BH. 1991.** Effect of bone distribution on vertebral strength: assessment with patient-specific nonlinear finite element analysis. *Radiology* **179:** 669–674.

Gans C. 1952. The functional morphology of the egg-eating adaptations in the snake genus Dasypeltis. *Zoologica* **37:** 209–244.

Giannini M, **Soares CJ**, **de Carvalho RM. 2004.** Ultimate tensile strength of tooth structures. *Dental Materials* **20:** 322–329.

Göçmen B, **Werner YL**, **Elbeyli B. 2008.** Cannibalism in *Dolichophis jugularis* (Serpentes: Colubridae): more than random? *Current Herpetology* **27:** 1–7.

Gunz P, **Mitteroecker P. 2013.** Semilandmarks: a method for quantifying curves and surfaces. *Hystrix, the Italian Journal of Mammalogy* **24:** 103–109.

Gunz P, **Mitteroecker P**, **Bookstein FL. 2005.** Semilandmarks in three dimensions. In: Slice DE, ed. *Modern morphometrics in physical anthropology.* New York: Springer, 73–98.

Herrel A, **Holanova V. 2008.** Cranial morphology and bite force in *Chamaeleolis* lizards–adaptations to molluscivory? *Zoology* **111:** 467–475.

Herrel A, **Vanhooydonck B**, **Van Damme R. 2004.** Omnivory in lacertid lizards: adaptive evolution or constraint? *Journal of Evolutionary Biology* **17:** 974–984.

Jackson K, **Underwood G**, **Arnold E**, **Savitzky AH. 1999.** Hinged teeth in the enigmatic colubrid, *Iguanognathus werneri*. *Copeia* **1999:** 815–818.

Jansen van Vuuren L, **Kieser JA**, **Dickenson M**, **Gordon KC**, **Fraser-Miller SJ. 2016.** Chemical and mechanical properties of snake fangs. *Journal of Raman Spectroscopy* **47:** 787–795.

Kardong KV. 1979. 'Protovipers' and the evolution of snake fangs. *Evolution* **33:** 433–443.

Kardong KV. 1980. Evolutionary patterns in advanced snakes. *American Zoologist* **20:** 269–282.

Kardong KV, **Young BA. 1996.** Dentitional surface features in snakes (Reptilia: Serpentes). *Amphibia-Reptilia* **17:** 261–276.

Kardong K, **Dullemeijer P**, **Fransen J. 1986.** Feeding mechanism in the rattlesnake *Crotalus durissus*. *Amphibia-Reptilia* **7:** 271–302.

Knox A, **Jackson K. 2010.** Ecological and phylogenetic influences on maxillary dentition in snakes. *Phyllomedusa: Journal of Herpetology* **9:** 121–131.

Koussoulakou DS, **Margaritis LH**, **Koussoulakos SL. 2009.** A curriculum vitae of teeth: evolution, generation, regeneration. *International Journal of Biological Sciences* **5:** 226.

Kroll JC. 1976. Feeding adaptations of hognose snakes. *The Southwestern Naturalist* **20:** 537–557.

Lawn BR, **Bush MB**, **Barani A**, **Constantino PJ**, **Wroe S. 2013.** Inferring biological evolution from fracture patterns in teeth. *Journal of Theoretical Biology* **338:** 59–65.

Lelièvre H, **Legagneux P**, **Blouin-Demers G**, **Bonnet X**, **Lourdais O. 2012.** Trophic niche overlap in two syntopic colubrid snakes (*Hierophis viridiflavus* and *Zamenis longissimus*) with contrasted lifestyles. *Amphibia-Reptilia* **33:** 37–44.

Losos JB, **Miles DB. 1994.** Adaptation, constraint, and the comparative method: phylogenetic issues and methods. *Ecological Morphology: Integrative Organismal Biology* **60:** 98.

Lucas PW. 2004. *Dental functional morphology: how teeth work.* Cambridge: Cambridge University Press.

Masschaele B, **Cnudde V**, **Dierick M**, **Jacobs P**, **Van Hoorebeke L**, **Vlassenbroeck J. 2007.** UGCT: new X-ray radiography and tomography facility. *Nuclear Instruments and Methods in Physics Research Section A: Accelerators, Spectrometers, Detectors and Associated Equipment* **580:** 266–269.

Nalla R, **Imbeni V**, **Kinney J**, **Staninec M**, **Marshall S**, **Ritchie R. 2003.** In vitro fatigue behavior of human dentin with implications for life prediction. *Journal of Biomedical Materials Research Part A* **66:** 10–20.

Platt DR. 1967. Natural history of the eastern and the western hognose snakes *Heterodon platyrhinos* and *Heterodon nasicus*. *University of Kansas Publications Museum of Natural History* **18:** 253–420.

Pregill G. 1984. Durophagous feeding adaptations in an amphisbaenid. *Journal of Herpetology* **18:** 186–191.

R Core Team. **2016.** *R: a language and environment for statistical computing*. Vienna: R Foundation for Statistical Computing. Available at: https://www.R-project.org/.

Rajabizadeh M. 2018. *Snake of Iran*. Tehran: Iranshenasi.

Rajabizadeh M, **Adriaens D**, **De Kegel B**, **Avci A**, **Ilgaz Ç**, **Herrel A. 2020.** Body size miniaturization in a lineage of colubrid snakes: implications for cranial anatomy. *Journal of Anatomy*. In press.

Rieppel O, **Labhardt L. 1979.** Mandibular mechanics in *Varanus niloticus* (Reptilia: Lacertilia). *Herpetologica* **35:** 158–163.

Savitzky AH. 1981. Hinged teeth in snakes: an adaptation for swallowing hard-bodied prey. *Science* **212:** 346–349.

Savitzky AH. 1983. Coadapted character complexes among snakes: fossoriality, piscivory, and durophagy. *The American Zoologist* **23:** 397–409.

Schlager S. 2013. Morpho: calculations and visualisations related to geometric morphometrics. R package v.0.23 3.

Schwenk K. 2000. *Feeding: form, function and evolution in tetrapod vertebrates*. Cambridge: Academic Press.

Terent'ev PV, **Chernov SA**, **Kockva L. 1965.** *Key to amphibians and reptiles*. Jerusalem: Program for Scientific translation [English translation of Opredelitel′ presmykayushchikhsya i zemnovodnykh, 1949].

Vlassenbroeck J, **Dierick M**, **Masschaele B**, **Cnudde V**, **Van Hoorebeke L**, **Jacobs P. 2007.** Software tools for quantification of X-ray microtomography at the UGCT. *Nuclear Instruments and Methods in Physics Research Section A: Accelerators, Spectrometers, Detectors and Associated Equipment* **580:** 442–445.

Waters N. 1980. Some mechanical and physical properties of teeth. In: Vincent JFV, Currey D, eds: *The mechanical properties of biological materials*. Cambridge: Cambridge University Press: 99–134. [Symposia of the Society for Experimental Biology, no. 34.]

Whitenack LB, **Simkins Jr DC**, **Motta PJ. 2011.** Biology meets engineering: the structural mechanics of fossil and extant shark teeth. *Journal of Morphology* **272:** 169–179.

Wiley DF, **Amenta N**, **Alcantara DA**, **Ghosh D**, **Kil YJ**, **Delson E**, **Harcourt-Smith W**, **Rohlf FJ**, **St John K**, **Hamann B. 2005.** *Evolutionary morphing*. Minneapolis: VIS 05 IEEE Visualization.

Zaher H, **Rieppel O. 1999.** Tooth implantation and replacement in squamates, with special reference to mosasaur lizards and snakes. *American Museum Novitates* **3271:** 1–19.

Zahradnicek O, **Buchtova M**, **Dosedelova H**, **Tucker AS. 2014.** The development of complex tooth shape in reptiles. *Frontiers in Physiology* **5:** 74.

Zhang Y-R, **Du W**, **Zhou X-D**, **Yu H-Y. 2014.** Review of research on the mechanical properties of the human tooth. *International Journal of Oral Science* **6:** 61.

SUPPORTING INFORMATION

Additional Supporting Information may be found in the online version of this article at the publisher's web-site.

Table S1. Bonferroni-corrected *P*-values resulting from the nonparametric multivariate analysis of variance on the landmark data of maxilla, palatine, pterygoid and mandible teeth in the examined snakes.

Table S2. Pairwise Euclidean distance along the centroid PC scores of the maxilla, palatine, pterygoid and dentary teeth